AIAA 2002-2472

Measurement of Trailing Edge Noise Using Directional Array and Coherent Output Power Methods

Florence V. Hutcheson and Thomas F. Brooks
NASA Langley Research Center
Hampton, VA 23681-2199

8th AIAA/CEAS
Aeroacoustics Conference
June 17-19, 2002 / Breckenridge, Colorado

For permission to copy or to republish, contact the copyright owner named on the first page.
For AIAA-held copyright, write to AIAA Permissions Department,
1801 Alexander Bell Drive, Suite 500, Reston, VA, 20191-4344.

AIAA-2002-2472

Measurement of Trailing Edge Noise Using Directional Array and Coherent Output Power Methods

Florence V. Hutcheson*
Thomas F. Brooks

NASA Langley Research Center
Hampton, Virginia 23681-2199

ABSTRACT

The use of a directional (or phased) array of microphones for the measurement of trailing edge (TE) noise is described and tested. The capabilities of this method are evaluated via measurements of TE noise from a NACA 63-215 airfoil model and from a cylindrical rod. This TE noise measurement approach is compared to one that is based on the cross spectral analysis of output signals from a pair of microphones placed on opposite sides of an airframe model (COP method). Advantages and limitations of both methods are examined. It is shown that the microphone array can accurately measures TE noise and captures its two-dimensional characteristic over a large frequency range for any TE configuration as long as noise contamination from extraneous sources is within bounds. The COP method is shown to also accurately measure TE noise but over a more limited frequency range that narrows for increased TE thickness. Finally, the applicability and generality of an airfoil self-noise prediction method was evaluated via comparison to the experimental data obtained using the COP and array measurement methods. The predicted and experimental results are shown to agree over large frequency ranges.

INTRODUCTION

Trailing edge (TE) noise has been an important subject of research for the past two decades because of its importance to airframe, broadband rotor and propeller noise. The noise source mechanisms at the trailing edge of an airfoil have been well studied and numerous mathematical approaches have been developed for the prediction of trailing edge noise [1]. The number of measurement methods developed for TE noise on an airfoil has been more limited. The main challenge, especially when testing in an open flow facility, has been to properly extract TE noise from extraneous noise sources. Schlinker [2] used a directional microphone utilizing an elliptic mirror, Yu and Joshi [3] used space-time correlation analysis, and Brooks and Hodgson [4] used a Coherent Output Power (COP) method to extract trailing edge noise of an airfoil from extraneous side-plates, nozzle, and open jet shear noise sources. The COP method used by Brooks and Hodgson was based on a cross-spectral analysis of pairs of output signals from microphones placed around the model airfoil. This COP method was also used by Gershfeld, et al. [5], along with statistical measurements of surface pressures and near-wake velocity profiles to quantify trailing edge noise for two-dimensional lifting airfoils. In the present paper, the use of a directional (or phased) microphone array for the measurement of trailing edge noise is presented.

Directional (or phased) microphone arrays can be used to localize noise sources by adjusting for propagation time delays from particular source locations to the microphones. Directional arrays are now frequently used for aeroacoustics measurements [6-13]. Their design and processing have been significantly improved since the 1970õ. In particular, acquisition and computational power has allowed increased array size (i.e., increased number of microphones) and better array designs. Improved

---

* Research Engineer, Aeroacoustics Branch, Member AIAA.
Senior Research Scientist Aeroacoustics Branch, Associate Fellow AIAA.

Copyright ' 2002 by the American Institute of Aeronautics and Astronautics, Inc. No copyright is asserted in the United States under Title 17, U. S. Government has a royality-free license to exercise all rights under the copyright claimed herein for government purposes. All other rights are reserved by the copyright owner.

signal-to-noise ratios have resulted through side lobe reduction. Graphical analysis presentation advances have greatly enhanced data interpretation and usefulness. A remaining challenge is the accurate measurement of the noise level produced by extended sources (such as TE noise) in the presence of compact sources. This problem has been pointed out by Mosher [14] and by Brooks and Humphreys [15]. A lot of the acoustic work that is currently being performed, use large arrays and processing methods that emphasise on strong localized sources and discriminate against distributed sources [16]. Brooks and Humphreys [15] have showed that the presence of spatially concentrated noise can interfere with distributed noise measurement. In some instances, the measured noise level from the extended source appears significantly lower than what it actually is. This problem becomes worse with increased array size.

This paper describes the approach and analysis that are used in an experiment study of trailing edge noise from a NACA 63-215 airfoil model. The model has been used previously as the main element in high-lift model testing [10, 12, 15, 17]. Far-field noise spectra and directivity from the trailing edge region of the airfoil are obtained. To better quantify the distributed noise source from the trailing edge of the model, the microphone array output from the standard beamforming technique [15] is used in a process to remove extraneous localized noise sources from the acoustic measurements. In the airfoil model testing, the effects of trailing edge geometry are examined. Also examined, by employing the same analysis procedures, is a cylindrical rod placed across the span and at the trailing edge position with the airfoil removed.

The results, obtained for the airfoil and rod test cases, using the array method are compared to those obtained using the COP method. Advantages and limitations of both measurement techniques are examined. The rod cases serve as an anchor for interpreting the measurement results. Finally, the results are used to examine the applicability and generality of the noise prediction method that was developed by Brooks et al. [18].

TEST SET UP

The trailing edge noise test was performed in the Quiet Flow Facility (QFF) of the NASA Langley Research Center. The QFF is an open jet facility designed for anechoic acoustic testing. A 2 by 3 foot rectangular open jet nozzle was employed. The model is a NACA 63-215 airfoil with a 16Ó chord and 36Ó span. For this normally flapped airfoil model, the flap was removed and the cut-out for the flap was filled in and contoured to render a spanwise uniform trailing edge region. The model (with flap) is shown mounted in the test section of the QFF in Figure 1. The model is supported above the nozzle by two side-plates that are mounted on the short sides of the nozzle.

Figure 1. Test apparatus with phased microphone array mounted on pivotal boom in QFF.

Treatments were applied to the trailing edge (TE) of the airfoil to modify the thickness and to model blunt trailing edges, with either square or rounded corners. As depicted in Figure 2, seven trailing edge configurations were examined with the level of thickness varying from 0.13Ó to 0.005Ó. Configuration #1 corresponds to the untreated airfoil trailing edge. Configuration #2 was obtained by tapping blue steel shim stock (0.005Ó thick) with 0.005Ó thick double-sided tape on the pressure side of the model, flushed with the TE, along the entire span of the airfoil. Configuration #3 was obtained by taping successively 0.035Ó thick rubber and 0.005Ó blue steel shim stock (using double-sided tape) also to the lower surface of the model and flushed to the TE. The increase in chord length of 0.043Ó was achieved by gluing a 0.075Ó thick wooden extension to the thickened TE. The added TE thickness in configuration #4 was achieved in the same manner as for configuration #3, but using 0.08Ó thick rubber instead. Configuration #5 was obtained by rounding off the corners (as described in Figure 2) of the wooden extension of configuration #3. Similarly, configuration #6 was obtained by gluing a 0.13Ó thick wooden extension with rounded corners to the TE described in configuration #4. Finally, configuration #7 was achieved by gluing a 0.005Ó thick aluminum tape extension to the upper surface of the airfoil TE. Clay

was used to provide a smooth transition surface for all TE treatments.

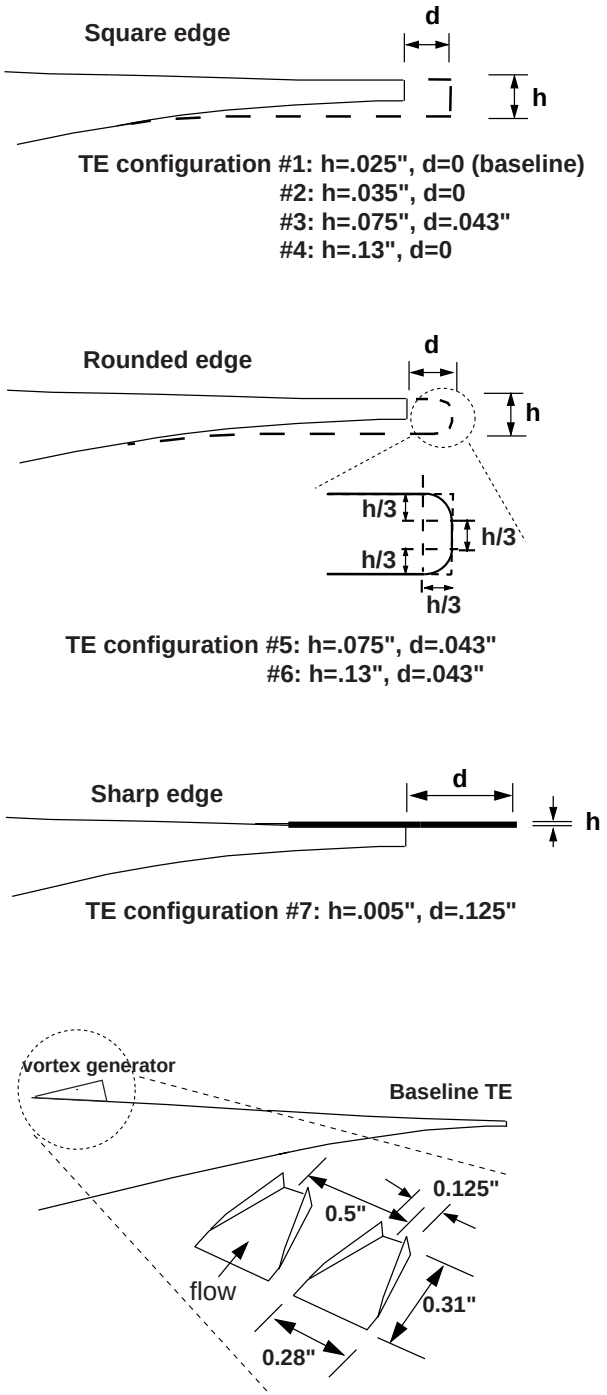

Figure 2. Airfoil TE configurations.

Grit, vortex generators or strips of serrated tape were used in certain configurations to trip the boundary layer. The airfoil's leading edge (LE) was alternatively wrapped over the entire span with a 1.625" wide strip of serrated aluminum tape or covered with #60 or #90 grit. These LE treatments covered the first 5 % chord region on the pressure and suction side of the model. For one of the airfoil configurations tested, in addition to the LE tape, another strip of aluminum serrated tape, 0.625" wide, was placed on the upper and lower surface of the model at 8% chord and a row of vortex generators was installed on the suction side at 85% chord. The vortex generators were placed 0.5" apart along the span of the model. Each vortex generator is made with 0.005" thick steel and is 0.31" long with a 0.28" wide base that narrows down to a 0.125" width at the top (see Figure 2). The sides of the device are fenced to a maximum height of 0.1".

The test conditions included mean flow Mach numbers up to 0.17 (corresponding to a wing Reynolds number up to about 1.7 million) and main element angles of attack ranging from —6.2 to 16 degrees. In this paper, only the results obtained with 0.17 mean flow Mach number and with the airfoil placed at —1.2¡ angle of attack (zero lift case) is presented. When referring to the pressure side of the model for the —1.2¡ angle of attack configuration, one will be talking about the "traditional" pressure side, i.e., the lower surface of the airfoil when at a positive angle of attack. Near wake velocity surveys were performed to determine the boundary layer/near wake thickness and displacement thickness at the TE of the airfoil. These measurements are used as inputs to the airfoil self noise prediction code (presented in a next section) to predict the noise radiated from the TE of the airfoil. The near wake velocity measurements are taken at about mid-span, 0.005" downstream of the airfoil's TE, along a line perpendicular to the plane containing the LE and TE of the model and extending 20mm above and below that plane. The measurements are made using a static pressure probe and a total pressure probe of 0.03" and 0.018" outside and inside, respectively.

For the rod test cases, the airfoil was removed from the test section and a rod was placed along what would have been the location of the trailing edge of the airfoil at —1.2¡ angle of attack. The diameter of the rods tested ranged from 0.0098" to 0.093" In certain configurations, grit was sprayed on the rods to trip the boundary layer. The same range of mean flow Mach numbers as in the airfoil test cases was considered. The results obtained with the clean ("untripped") 0.093" diameter rod will be presented.

The Small Aperture Directional Array (SADA) [12, 15, 17] used to measure the far field acoustics

consists of 33 B&K 1/8Ó microphones projecting from an acoustically treated frame. The microphones are arranged in 4 co-centric irregular rings of 8 microphones each with one microphone at the center of the rings. Each ring is twice the diameter of the ring it encloses, the diameter of the outer ring being 7.78Ó Thus, the aperture of this microphone array is small, ensuring that all the microphones lie within approximately the same source directivity. This directional array is mounted on a pivotal boom and can be readily moved around the model to different elevation angles Φ as depicted in Figures 1 and 4. For the present test, the array is located approximately five feet from the center of the airfoil trailing edge. Because of the two-dimensional nature of the model under investigation, SADA measurements were made only in the plane perpendicular to the TE at the span centerline.

Two additional microphones (microphone #34 and #35) were also placed in the noise field on either side of the model out of the flow (see Figure 4). These two microphones were used in previous airframe noise studies [10, 12] to provide reference signals. Their location was not modified for the present test and their output signals were used to measure the noise radiated from the trailing edge of the airfoil and from the rod using the COP method.

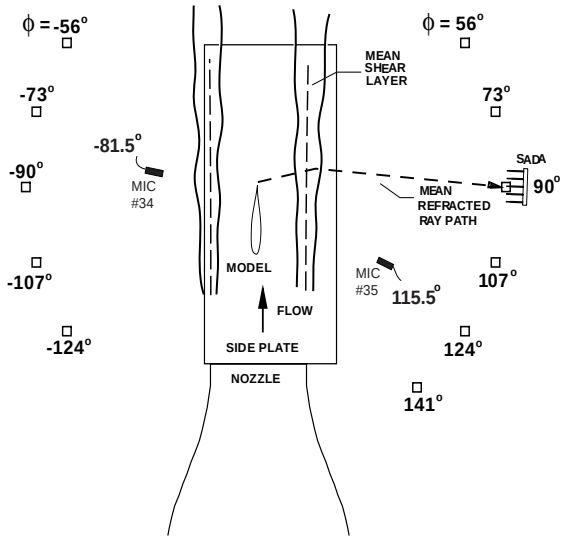

Figure 4. Sketch of the test set up with microphones locations and elevation angles.

Data Acquisition and Processing

Two transient data recorders (NEFF) controlled by a workstation were used for the data acquisition. The data from all 35 channels were recorded simultaneously at a sampling rate of 142.857 kHz and with a dynamic range of 14-bit. A high pass and a low pass filter set respectively at 300 Hz and 50 kHz were used to condition the outputs from each microphone channel. Piston-phone and injection calibrations of amplitude and phase were made for each microphone of the array (see references 10, 12, 15, and 17).

The first step of the post processing involves the construction of the cross-spectral matrix for each set of data acquired from the 35 microphones channels. Individual elements of the cross-spectral matrices were computed by partitioning each time signal into 1000 non-overlapping segments of 2^{13} samples. Each time history segment was then Fourier transformed using a Hamming window for signal conditioning. The resulting frequency resolution was 17.45 Hz. The cross and auto-spectra were obtained from the following equation:

$$G_{ij}(f) = \frac{1}{NW_H} \sum_{k=1}^{N} \left[X_{ik}^{*}(f)\, X_{jk}(f) \right] \qquad (1)$$

where i=1,É35 and j=1,É35. $G_{ij}(f)$ are the elements of the cross-spectral matrices **G**, W_H is the weighting constant corresponding to the Hamming window, N is the number of time history segments (i.e., N=1000), X represents a fast Fourier transform data segment and * indicates complex conjugate. The cross-spectral matrices, **G**, are used to obtain power spectra from noise source locations of interest. This is described in the next section.

ANALYSIS METHODOLOGIES

Microphone Array Method

Conventional frequency domain beamforming [19] is used to electronically Òsteer Ó the SADA to chosen noise source locations. For each selected steering locations a steering vector **e** containing an entry for each microphone in the SADA is constructed [17]:

$$\mathbf{e} = \left[A_i \exp\left\{ -j\left(\vec{k}.\vec{x}_i + \omega \Delta t_i \right) \right\} \right]_{i=1,33} \qquad (2)$$

where $\vec{k}$ is the local wavenumber vector, $\vec{x}_i$ is the distance from the steering location to each microphone of the array. A_i and $\omega \Delta t_i$ are, respectively, the amplitude and phase correction for microphone i to

account for the refraction of sound transmission through the shear layer. The correction calculations as described by Humphreys, et al.[17] are based on Amiet's method [20], with modifications made to account for a curved three-dimensional mean shear layer surfaces. The array output power spectrum at a steering location is obtained from

$$p(\mathbf{e}) = \frac{\mathbf{e}^T \mathbf{W}\left(\mathbf{G} - \mathbf{G}_{background}\right)\mathbf{W}^T \mathbf{e}}{\left(\sum_{i=1}^{33} w_i\right)^2} \qquad (3)$$

where the superscript T indicates complex transpose and $\mathbf{G}_{background}$ is the cross-spectral matrix obtained from the data acquired when no model is present in the test section. This background subtraction process is performed to reduce noise contamination from extraneous sources such as noise emanating from the lip of the nozzle, from the side-plates or any other aperture present near the test section. **W** is a frequency-dependent weighting-function row matrix containing the w_i weighting coefficients that are used to shape the array response.

Array characteristics. In Eq. (3), **W** is defined in such a way that keeps the array beamwidth approximately invariant with frequency between 10 and 40 kHz [17]. The "beamwidth" (i.e., spatial resolution) of the microphone array is defined as the width across the main response lobe over which the sensing level is within 3 dB from the peak level. Between 10 and 40 kHz the SADA beamwidth is equal to approximately 1 foot and below that frequency range it increases as the frequency decreases (and above that range, decreases as frequency increases). Thus, at about 3.15 kHz, the beamwidth of the array is close to 3 feet wide, covering the entire span of the model.

To demonstrate the functioning of the microphone array, results are shown in Figure 5 for a calibrator source that is placed in the flow at mid-span just above the airfoil TE. The calibrator source is the open end of a 1" diameter tube mounted to an out-of-flow acoustic driver. The source is flush with the vertical plane containing the chordline of the airfoil. The input signal to the driver is white noise. Acoustic measurements on the pressure side of the model are taken with the SADA located at an elevation angle of 90° and aligned with the center of the trailing edge of the airfoil. The acoustic field contour map presented in Figure 5 was obtained by steering the array over the vertical plane containing the trailing and leading edges of the airfoil. The flow is from bottom to top in the figure. At any point on the contour plot, the levels shown represent the output of the array when the array is steered (while accounting for shear layer refraction as per Eqs. (2) and (3)) to the point.

It is seen in Figure 5 that the array accurately locates the calibrator source and that the noise level falls when the array is electronically steered away from the calibrator source location. The measured peak level being 81 dB, this noise map indicates that the beamwidth of the array at 8 kHz is about 14".

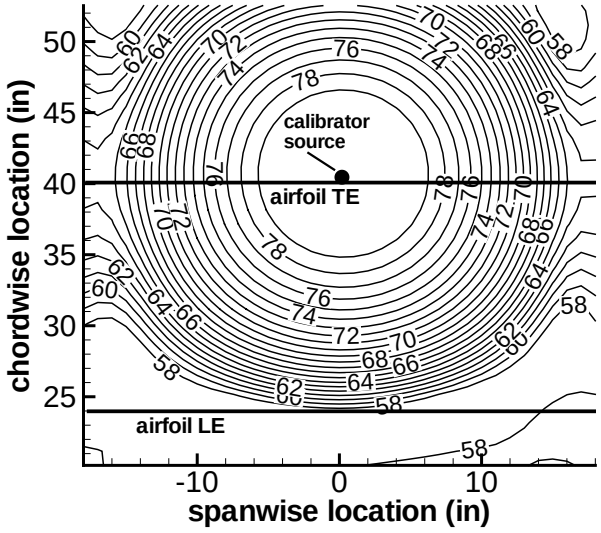

Figure 5. Noise source distribution contours over the pressure side of the airfoil at —1.2 angle of attack with a calibrator source located on the TE at mid-span. M=0.17, SADA elevation angle ϕ = 90°. One-third octave levels for $f_{1/3}$ = 8 kHz.

By reciprocity, the spatial attenuation (or beam) pattern of the SADA can be determined from the response contours obtained from the calibrator source test. Any lack of perfect symmetry is due to the airfoil / side-plate reflections. The result for 8 kHz of Figure 5 is contained in Figure 6. Array beam patterns are displayed in Figure 6 for the 3.15, 6.3, 8, 12.5, 20 and 31.5 kHz one-third octave bands. Each plot covers a 5" by 5" planar area centered at the calibrator source and containing the LE and TE of the airfoil. The noise maps, showing the array main lobe characteristics and location of the side lobes, define how the array spatially discriminates against noise source regions. If one steers to other locations, the attenuation patterns will shift along with the steering.

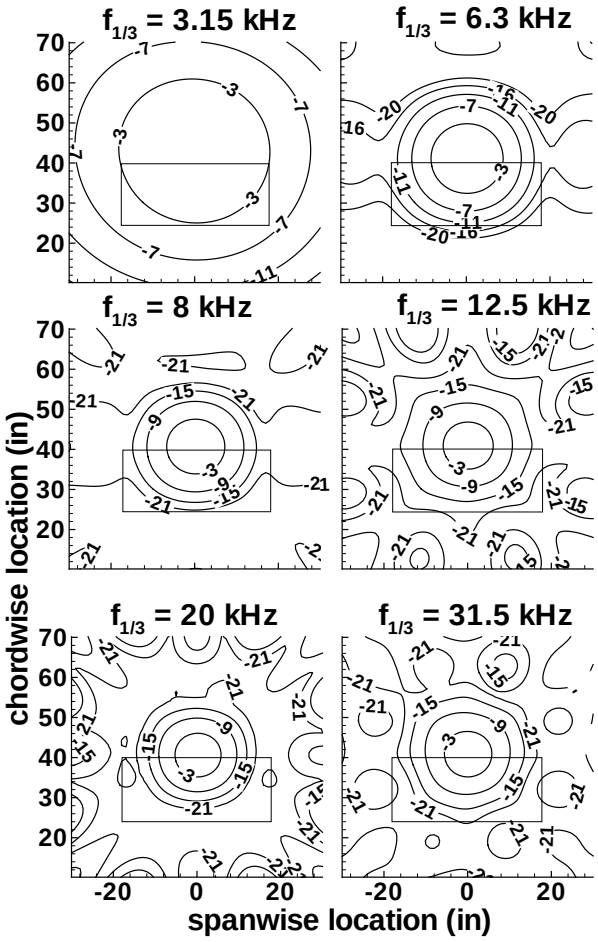

Figure 6. SADA beam pattern from the calibrator source.

Distributed source characteristics. Figure 7 shows a contour map corresponding to that of Figure 5, except that the source is removed from the vicinity of the model's TE. The contour levels are seen to drop substantially to reveal the generally uniform distribution of TE noise across the model span. Note the general two-dimensional fall-off in level away from the TE. But, this is interrupted by regions of higher localized noise levels near the model airfoil/support side-plate junctions. This contour characteristic is observed over a large range of frequencies for a number of test conditions.

Figure 8 shows the map obtained if the airfoil model is replaced by a 0.093" diameter rod. The rod is positioned where the airfoil trailing edge was previously located. It is seen that the array successfully captures the strong two-dimensional characteristic of the noise radiated by the rod. The slight drop off in level for the array result at the side-plates is expected (because then only part of the beam pattern includes the distributed noise source) for a uniform source distribution that terminates at the span edges. Note that any rod / support side-plate noise (prominent for TE noise in Figure 7) is submerged below the much higher levels of the rod at this frequency.

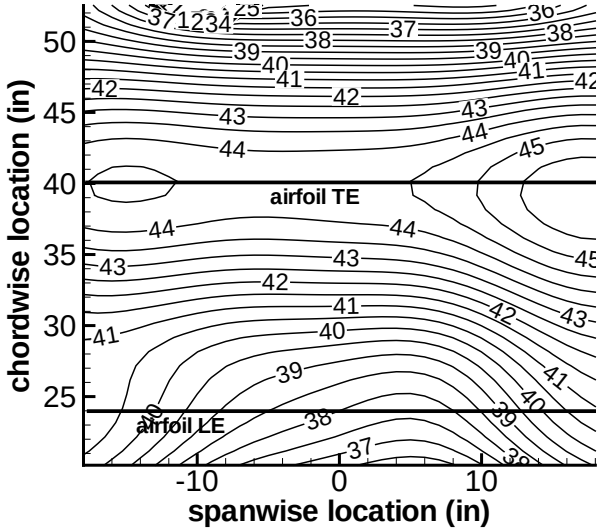

Figure 7. Key per Fig. 5 but that the source is removed to reveal model TE noise. TE configuration #1 and #90 grit on the leading edge. $f_{1/3}$ = 8 kHz.

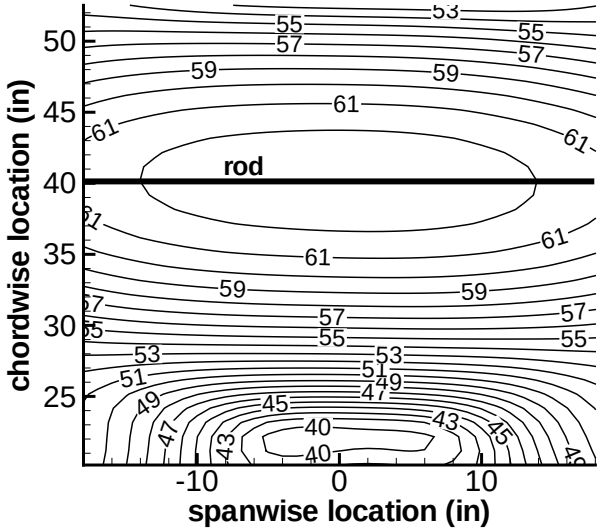

Figure 8. Noise source distribution contours for a 0.093" diameter rod. M=0.17 and SADA elevation is 90°. One-third octave levels for $f_{1/3}$ = 8 kHz.

Per foot spectra calculations. It was desired to produce an easily interpreted spectral presentation of TE noise and rod noise from the noise measurements. The chosen presentation is that of noise spectra due to a one-foot span of uniformly distributed TE noise (or rod noise) for an observer five feet away. A processing procedure was developed that is explained in more detail in Mendoza, et al. [21], who applied it to the slat noise problem. As indicated in Ref. 21, the integration method of Brooks, et al. [15] could have been adapted to the problem. However, a simpler, more direct, method is used for the particular problem of this paper. It is summarized here.

The procedure is intended to determine spectra on per foot basis while minimizing any extraneous contributions such as from the junction regions of the model and the side-plates. Figure 7 is an example where these contributions are locally more intense than the distributed TE noise sources. The method follows:

(i) The noise level measured by the array steered to the mid-span point of the TE is assumed to be exclusively due to the distributed source. For each array location considered, spectra are computed using the "standard" array processing described earlier.

(ii) The amplitude of each spectrum is adjusted as a function of frequency by a function F. The function F is the ratio of the noise that would be perceived by a single microphone placed at the SADA location from a one-foot wide uniform distribution of incoherent noise sources, centered at mid-span, and the noise that would be perceived by the array from a similar source but distributed over 3.25 feet. F is frequency dependent and is calculated for each array location considered. The extra 0.25 feet in span are added to approximately account for reflections in the side-plate regions.

The spectra adjusted by F thus represents a measure of the TE noise (or rod noise) alone, on a per foot basis (i.e., TE noise spectra generated by an airfoil of 1 foot span).

COP Method

The technique used in this study to measure TE noise from cross-spectral analysis of pairs of microphone signals was developed by Brooks and Hodgson [4] and is consistent with the general coherent output power (COP) definition given by Bendat and Piersol [22]. This noise measurement method is based on the conceptual model that TE noise is an edge pressure scattering phenomenon that has a dipole character, where the axis of the dipole is perpendicular to the mean flow and to the TE of the model. Thus, the TE noise spectrum S(f) that would be measurable and coherent at both microphones #34 or #35, is computed from

$$G_{34,35}\ \exp\{i[\pm\pi + k(R_{35} - R_{34})]\} \qquad (4)$$

where $G_{34,35}$ is the cross-spectrum between the signals received by microphones 34 and 35, k is the local wave number and R_{34}, R_{35} are the distances from the airfoil TE (or from the rod) to microphones 34 and 35, respectively. The exponential in Eq. (4) serves to remove the phase offset that occurs when $R_{34} \neq R_{35}$. The use of this cross-spectral approach has the advantage that only correlated noise is retained by $G_{34,35}$. Extraneous and uncorrelated noises received by microphones 34 and 35 are mutually incoherent and are thus excluded.

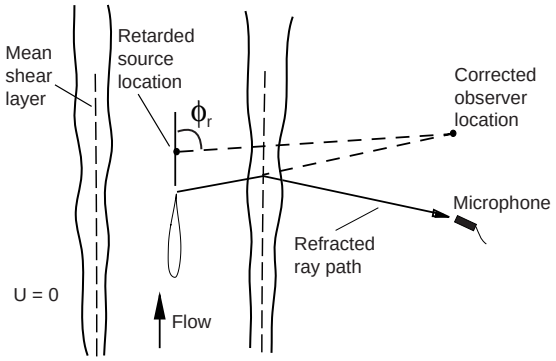

Figure 9. Sketch of shear layer refraction of acoustic ray paths.

For cases where $R_{34} = R_{35}$ and the microphone elevation angles are +/- 90°, the TE noise spectrum S(f) $=|G_{34,35}|$. However, microphones 34 and 35 are located, respectively, on opposite sides of the model at -81.5° and 115.5° elevation angles, 23.8 and 31.5 inches from the airfoil TE and in a plane perpendicular to the model, 11" from mid-span. The analysis used to determine S(f) accounts for the fact that the two microphones are not located symmetrically and are not placed far enough from the distributed source to observe every segment of the source from approximately the same distance. To facilitate comparison between the measurements and predictions, S(f) is put on the same basis of an observer 5 feet from a 1 foot span source. In the analysis, the following radiation directivity patterns are assumed [14]:

$$D_a(\phi) = \frac{2\sin^2(\phi_r/2)}{(1+M\cos\phi_r)[1+(M-M_c)\cos\phi_r]^2} \qquad (5)$$

for the noise radiating from the airfoil TE, and

$$D_r(\phi) = \frac{\sin^2(\phi_r)}{(1+M\cos\phi_r)^2} \qquad (6)$$

for the noise radiating from a rod. In Eqs. (5) and (6), ϕ_r (see Figure 8) is expressed in the retarded coordinates system [20], M is the free stream Mach number and M_C (~ 0.6 M) is the convection Mach number assumed for turbulence convecting pasting the airfoil TE.

Finally, it should be pointed out that the COP method used here for TE noise (or rod noise) is much more restrictive in application than are array methods. Experience has found that applying the method to cases were multiple sources or source lines (for example, with different R_{34} and R_{35} values) are present, the method can become intractable unless source modeling and separation methods of some ingenuity are used.

Comparative Prediction Method

The airfoil self-noise prediction method compared to data is from Brooks, et al. [18]. It is a semi-empirical model based on data acquired from aeroacoustic experiments by Brooks, et al [4, 23, 24, 25] using two and three-dimensional NACA 0012 airfoil sections of different chord lengths, angles of attacks, Reynolds numbers, and subsonic Mach numbers. Five self noise mechanisms were identified and modeled: boundary-layer turbulence passing the trailing edge (TBL-TE noise), separated boundary layer and stalled airfoil flow, vortex shedding due to laminar boundary layer instabilities (LBL-TE noise), vortex shedding from blunt trailing edges (BTE noise), and airfoil tip turbulent vortex flow. Of these only the TBL-TE, LBL-TE, and BTE noise sources have pertinence to the present problem of a two-dimensional airflow at —1.2… angle of attack.

Since the airfoil used in the present study (NACA 63-215) is different from the one used to develop the airfoil self-noise prediction code, the actual thicknessδ and displacement thickness δ^* of the boundary layer at the TE of the airfoil were measured for the different angles of attack and types of boundary layer tripping treatment tested. In most cases, these were used in the prediction code instead of the values calculated internally by the code. The measured thickness values and the corresponding values calculated from theory for a symmetrical (NACA 0012) airfoil are shown in Table 1 for the cases considered here.

Table 1. Predicted and measured boundary layer thickness values (M=0.17, AOA= -1.2¡)

	Predicted (mm)			Measured (mm)		
LE treatment	δ_p	δ_p^*	δ_s^*	δ_p	δ_p^*	δ_s^*
No treatment	7.3	1.9	1.2	10.3	1.4	1.2
Serrated tape	4.4	2.8	1.7	8.5	2.5	2.3
#90 grit	7.3	4.8	2.9	15.2	3.5	2.8

RESULTS

Measurements and Processing Method Comparisons

Noise contours. In Figure 9, noise contour maps from array measurements for the smooth 0.093Ó diameter rod are shown. The conditions are the same as in Figure 8, with the plane scanned by the microphone array the same as that for the airfoil in Figure 7. It is seen that the noise radiation exhibits strong two-dimensional behavior for all one-third octave frequency bands from 3.15 to 20 kHz. This was found true through the 40 kHz band (not shown here).

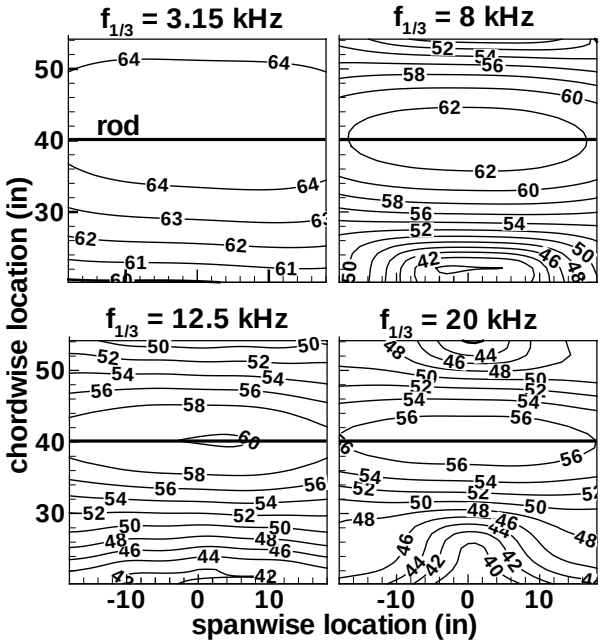

Figure 9. Noise source distribution contours for a 0.093Ò diameter rod. M=0.17 and SADA elevation is 90°. One-third octave presentation.

Contour maps for the airfoil model at —1.2… angle of attack are shown in Figure 10 for four one-third octave frequency bands. These were obtained in the manner of Figure 7. The LE of the model was covered with boundary layer tripping #90 grit and the trailing edge thickness was 0.005Ó(TE configuration #7).

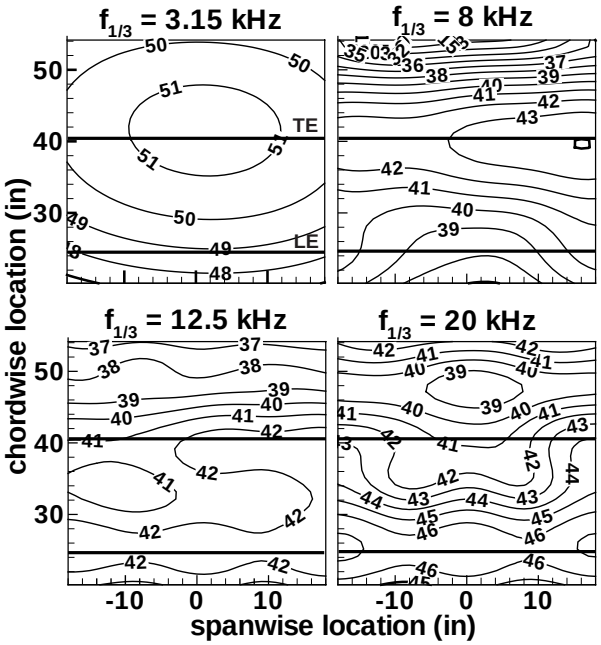

Figure 10. Noise source distribution contours over the Òpressure Óside of the airfoil at —1.2° angle of attack. M=0.17 and SADA elevation is 90°. The TE configuration is #7 and #90 grit on LE. One-third octave presentation.

It is seen that the two-dimensional characteristic of the noise radiating from the TE is well captured by the array for the 3.15 and 8 kHz one-third octave bands. For higher frequency bands, noise radiating from the #90 grit boundary layer tripping placed along the LE of the airfoil (rendering Òscrubbing Ótype noise) and from the side-plate junction regions becomes important. At 12.5 kHz, the noise levels radiated from the LE more than equal those from the TE. At 20 kHz, the LE levels totally dominate, thereby Òmasking Óthe noise radiated from the airfoil TE. In fact, any two-dimensional noise (contour) character near the TE has disappeared — indicating that the levels one obtains when focusing there are due primarily to LE and other extraneous (with respect to the TE noise) noise through side lobe communication illustrated in Figure 6.

A point to remember, in assessing relative levels and discrimination between source contributions, is that a level recorded at any point is due the integration of noise from all regions through the beam pattern spatial weighting shown in Figure 6. Referring to the 20 kHz case in Figure 6, the attenuation from a focus at the TE to the LE region is about 21 dB. In Figure 10, the difference in level between the LE and TE regions are only 4 to 5 dB. Simple calculations can clearly show that the integration effect easily accounts for this smaller measured difference at the TE. This integration effect can be even more of a problem for different array sizes and source types, as studied by Brooks, et al.[15].

In one sense, the high frequency array results for the airfoil are very successful. The array successfully captures the two-dimensional characteristic (and the quantitative spectrum) of the noise radiating from the LE. The COP method totally fails to measure this noise because this grit-related noise is incoherent with that radiated to the other side of the airflow — so there is no correlation between microphones. Therefore the array can define the total noise from a surface, while the COP method is set up to measure only that noise that meets the COP-method assumptions.

Spectral presentations. The unadjusted (standard SADA processing) spectrum measured with the SADA at the center of the rod is shown in Figure 11, along with the adjusted per foot spectrum obtained with the noise extraction procedure described earlier. It is observed that levels from the two spectra differ significantly only below 10 kHz, where the main lobe beamwidth of the array is larger than 1 foot. (The per foot procedure, as previously described, corrects the levels to what they would be if one were measuring, with a single microphone, a source with a 1-foot span.) The same observation can be made for the TE noise and LE noise spectra displayed in Figure 12 for the airfoil test case. These spectra were obtained by electronically steering the SADA respectively to the center of the airfoil TE and alternately to the center of the airfoil LE. A non-discriminating evaluation of the results of Figure 12 would perhaps lead one to the belief that below 3 kHz, the LE radiates noise as strongly as the TE, which is incorrect. Such interpretation concerns were discussed above for Figure 10 and shows that contour plots can be an invaluable diagnostics.

The per foot spectrum obtained for the rod from SADA measurements is compared in Figure 11 to the corresponding spectrum determined from the COP method. The agreement between results, from the two quite distinct methods, is very good between 2.5 and 8 kHz. The accuracy of the SADA measurements below 1 kHz is questionable because of the very large beamwidth of the array for that frequency range (making the array more omni-directional and thus

measuring everything). However, as shown in Figure 9, the SADA captures the strong two-dimensional nature and high level of the distributed noise source over the rest of the frequency range considered. This means that the spectrum obtained with the SADA should give an accurate representation of the actual noise level from the distributed source above about 1 kHz.

The phase of the cross-spectrum calculated between microphones 34 and 35 for the COP method is shown in Figure 12. Included also in Figure 13 are the one-third octave phase values as determined by vectorial summation of the cross-spectral narrowband components. This improves the statistics of the phase definition.

From Figure 12, it is seen that the assumption that the noise emanating from the rod radiates like a dipole holds only between 2.5 kHz and 8 kHz (i.e., where the phase remains around 180 deg). Below or above this frequency range, this assumption fails and the noise levels calculated with the COP method are not necessarily representative of the noise radiating from the rod. It is also shown in Figure 12 that the narrowband phase of the cross-spectrum begins to scatter (randomize) around 7 kHz. This is seen, in Figure 11, to correspond to the frequency range where the spectra measured with the COP method and SADA array begin to differ.

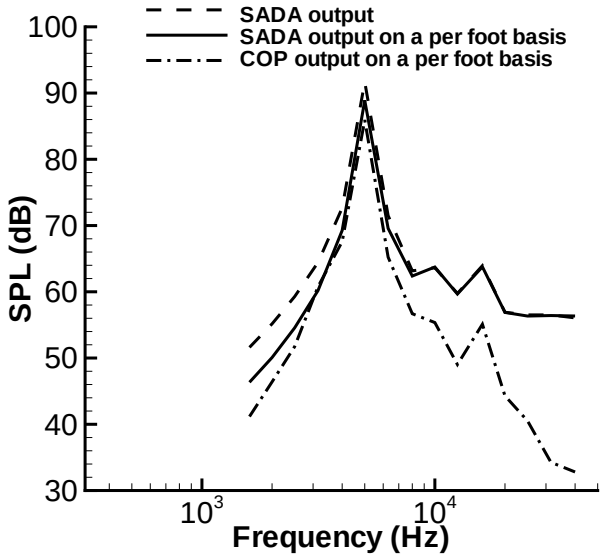

Figure 11. Comparison between the COP and array based noise measurement methods for the rod case of Fig. 9. The array scan point is on the rod at mid-span.

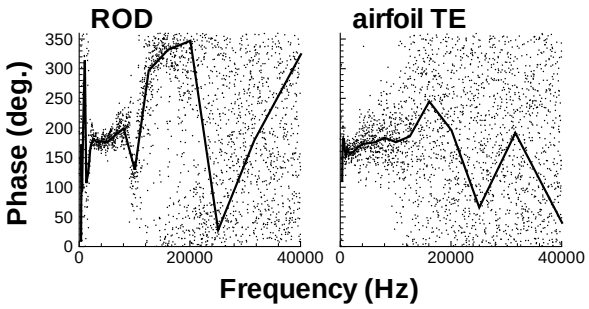

Figure 12. Phase of cross-spectra between signals of microphones 34 and 35 used in the COP method. The phases are corrected to account for location of microphones 34 and 35 and the shear layer corrected ray path.

Similarly, in Figure 13 for the airfoil test case, the spectra obtained with the COP and the SADA array method compare well between 700 Hz and 7 kHz, but differ by up to 10 dB at lower and higher frequencies. It is seen in Figure 12 that the phase of the cross spectrum remains around 180° between 700 Hz and 12.5 kHz when its value is averaged over one-third octave bands. However, on a narrowband basis, the phase increasingly scatters above 4 kHz, suggesting a drop in coherence level due to a reduced signal to noise ratio. The summing of narrowband cross-spectral (vectorial) components diminishes levels appropriately in the forming of one-third octave levels. Below 700Hz and above 12.5 kHz, the dipole assumption on which the COP method is based fails and hence the measurement method is no longer valid.

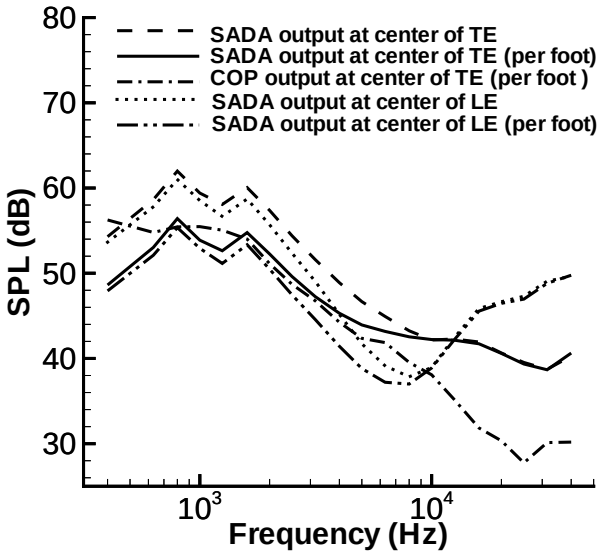

Figure 13. Comparison between the COP and array based noise measurement methods for the airfoil case of Fig. 10. The array scan point is first at center of TE then at center of LE.

The disagreement between the SADA and COP measurements above 10 kHz is further increased because of the strong noise radiation from the LE grit. As mentioned previously, the TE noise levels measured with the directional array above 10 kHz are higher than they would otherwise be because of side lobe contamination from the LE region. For this specific airfoil configuration, the COP and the SADA directional array measurement methods for TE noise both fail above 10 kHz, and results are also questionable for the very low frequency range. However, for the rod case, where the signal measured by the array main directional lobe is strong for all frequencies and side lobe contamination is minimum, the SADA performed well and can be believed over most of the frequency range.

TE Noise Spectra and Comparisons to Prediction

The TE noise spectra obtained using the COP and the SADA array method for different airfoil TE configurations are presented in Figure 14, along with the spectra obtained from the airfoil self noise prediction method. For these test cases, the LE of the airfoil was covered with #90 grit. The frequency range for which the SADA and the COP measurements are believed to be valid (based on concerns stated above and processed data not shown) is indicated in each plot. Also indicated is the predicted peak frequency corresponding to the TE bluntness noise.

As indicated for TE configurations #1, 2, and 7, the TE noise levels measured by the SADA should be accurate between 1 and 10 kHz. For the other TE configurations examined, the valid frequency range is reduced to 1 to 8 kHz. It was observed from contour maps for the 8 to 10 kHz frequency range, noise emanating from the .005Ó.025Óand .035Óthick trailing edges radiated more strongly than from the thicker TE tested. Thus at 8 kHz, the TE noise levels measured by the SADA (at the center of the TE) is 44.5 dB for a TE thickness of 0.025Óand 37.5 dB for a TE thickness of and 0.13Ó At 10 kHz, TE noise dominates the noise radiating from LE grit only for the cases with TE thicknesses of .005Ó.025Óand .035ÓFor the other TE configuration tested LE noise was dominant. Hence, it was concluded that for the three thinnest TE configurations considered (i.e., conf. #1, 2 and 7), the TE noise levels measured by the SADA should be accurate in the frequency range of 1 and 10 kHz. For the thicker TE configurations examined, that frequency range reduces to 1 to 8 kHz. Measurements below 1 kHz are rejected because of the very large array beamwidth at these low frequencies. Note that the use of a rounded versus square TE had no significant effect on the TE noise levels.

Similarly for the COP method, it was determined by examination of the phase behavior that the COP results represent a good measure of TE noise up to 7 or 8 kHz for TE configuration #1, 2, and 7, and only up to 5 kHz for the other TE configurations. Above these frequencies, the phase scatter became significant and the dipole radiation assumption began to fail. One possible contribution to the rapid deterioration of results obtained with the COP method for the thick trailing edges is the departure from the assumption that the measured noise radiated from a point (or line) dipole. Thus as the TE thickness increased, the phase scatter increases adding at least some negative bias to the measurements. This adds to the drop in the measured sound pressure levels above 5kHz.

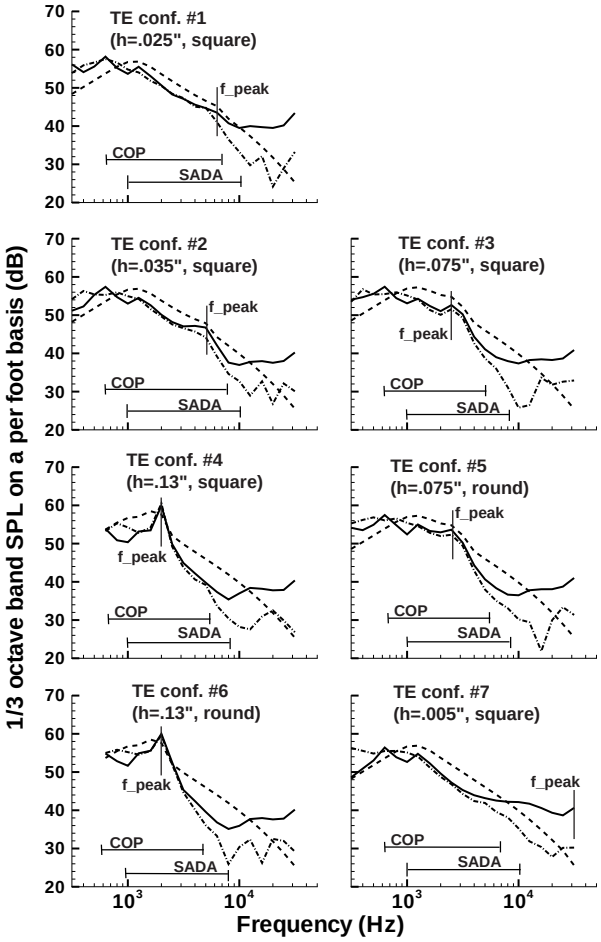

Figure 14. One-third octave band TE noise spectra (per foot). M=0.17, angle of attack = -1.2°, #90 grit on LE.
– – – – – prediction, —·—·— COP output, ——— array output (SADA at 90° elevation angle).

Prediction comparisons. At —1.2 angle of attack, the airfoil self-noise mechanisms that dominate the TE noise spectra are TE bluntness (BTE noise), boundary-layer turbulence passing the trailing edge (TBL-TE noise) and vortex shedding from a laminar boundary layer (LBL-VS noise). For the measured results presented in Figure 14, the boundary layer was fully tripped on both sides of the airfoil, therefore BTE and TBL-TE noise dominates. The peaks that are related to TE bluntness are well predicted. These peaks are less pronounced as the TE thickness decreases. The predicted amplitude and frequency of these spectral peaks are very sensitive to the value given to the parameter ψ used in the prediction code to incorporate effects from the TE geometry. (This parameter is also reflective of the solid angle between the airfoil surfaces immediately upstream of the TE. In Ref. 18, ψ = 14… for the NASA 0012 TE thickness). Figure 15 shows the variation of the predicted TE noise spectra for three values of ψ. It is seen that with decreasing values of ψ, the spectral peak amplitude and frequency increase. A value of ψ = 20° was used for the prediction in the present study because it gave reasonable prediction-data comparisons for all the test cases of different thicknesses examined.

It is observed that for frequencies larger than the BTE peak frequencies, the predicted TE noise levels are higher than the ones that are believed to be accurately measured by the SADA and COP methods. The prediction assumes an independent summation of the BTE noise due to a TE of finite thickness with the TBL-TE (and/or LBL-VS) noise from a sharp TE airfoil. The measured TE noise data suggest that the two effects may not be independent, affecting the noise levels at higher frequencies.

For some of the airfoil configurations tested, it is seen in Figure 14 that TE noise was under-predicted below about 1 kHz. Using the boundary layer thickness parameters calculated by the code (based on a symmetrical NACA 0012 airfoil) appeared to improve the prediction in the low frequency range of the spectra for these test cases. This is shown for example in Figure 16 for TE configuration #5. However, because of the questionable accuracy of the SADA array and COP measurement methods below 1 kHz (large array beamwidth and failed dipole-like radiation assumption), it is difficult to say whether using the predicted or measured boundary layer thickness values led to better prediction results. The measured values are used in other figures.

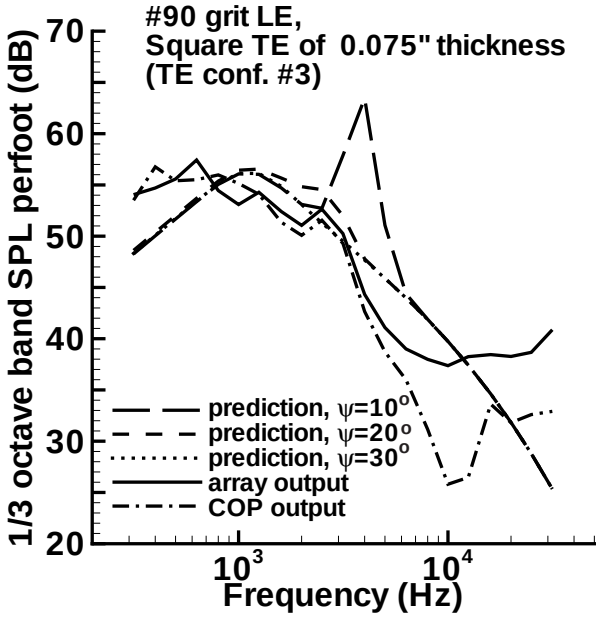

Figure 15. TE noise spectra predicted using measured boundary layer thickness and displacement thickness. Comparison to measured TE noise spectra. M=0.17 and airfoil is at —1.2 angle of attack. #90 grit on LE, with TE configurations #3 and 5.

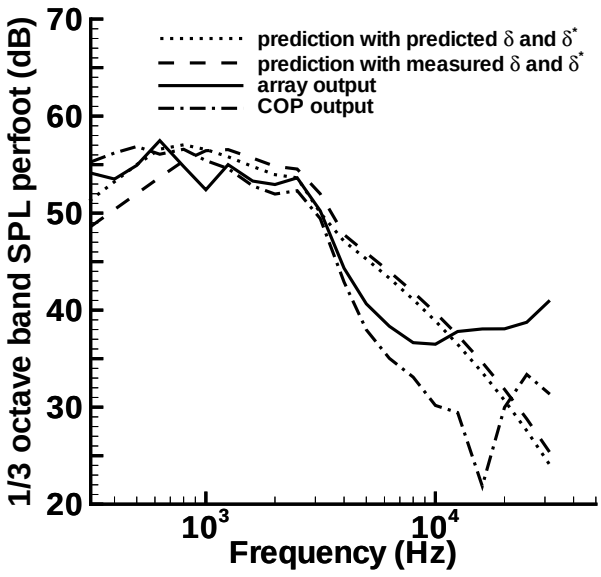

Figure 16. TE noise spectra predicted with or without using measured boundary layer thickness and displacement thickness. Comparison to measured TE noise spectra. M=0.17 and airfoil is at 1.2° angle of attack. #90 grit on LE and TE configuration #5.

The TE noise spectra obtained using the COP and SADA array methods for different boundary layer tripping treatments are presented in Figure 17 along with prediction results. The frequency range for which SADA and COP measurements are believed to be valid is also indicated. For each of the test results presented below, the baseline trailing edge configuration #1 was used.

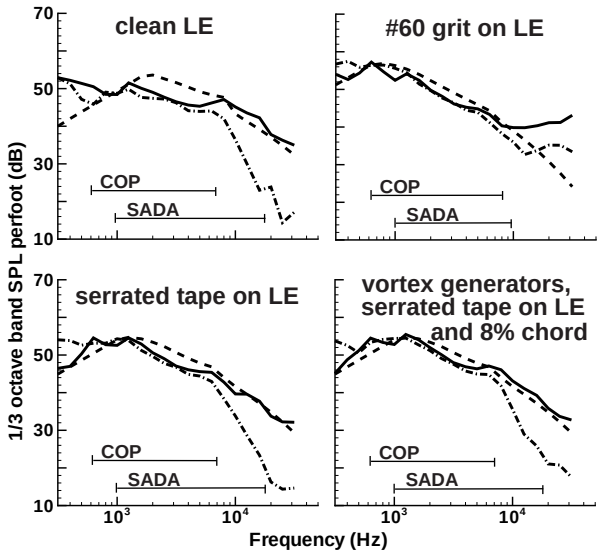

Figure 17. Comparison of predicted and measured TE noise spectra. M=0.17 and airfoil is at —1.2 angle of attack. Baseline TE configuration #1. – – – – Prediction, —·—·— COP per foot output, ——— array per foot output (SADA at 90° elevation angle).

As indicated for the #60 grit LE treatment case, the TE noise levels measured by the SADA should be valid between 1 and 10 kHz. As was found for the # 90 grit LE treatment, the #60 grit was a strong radiator and dominated other noise sources above 10 kHz, thereby contaminating TE noise measurements. Other LE treatments were weak radiators, minimizing side lobe contamination. In these cases, however, the boundary layer was not fully tripped and there were indications of other noise sources present near the airfoil TE region at and above 20 kHz. This likely raised the sound pressure level of the TE noise spectra measured with the SADA by a few decibels above 20 kHz.

Directivity

The TE noise spectra obtained with the SADA located at different elevation angles are shown in Figures 18 and 19 for the airfoil configuration #7 and for the 0.093Ódiameter rod, respectively. Eqs. (5) and (6), respectively, were used to scale the airfoil and rod spectra. The airfoil TE noise spectra are seen to collapse between 1.5 kHz and 12.5 kHz, apparently confirming that the SADA successfully measures TE noise within that frequency range. Above 12.5 kHz, the spectra do not collapse supporting the finding that for this airfoil configuration, the higher frequency part of the spectra is not representative of TE noise but includes extraneous noise sources due to side lobe contamination. Also note that the spectra obtained with the SADA at the highest (–56¡) or lowest (141¡) elevation angles, did not collapse as well as the rest of the spectra.

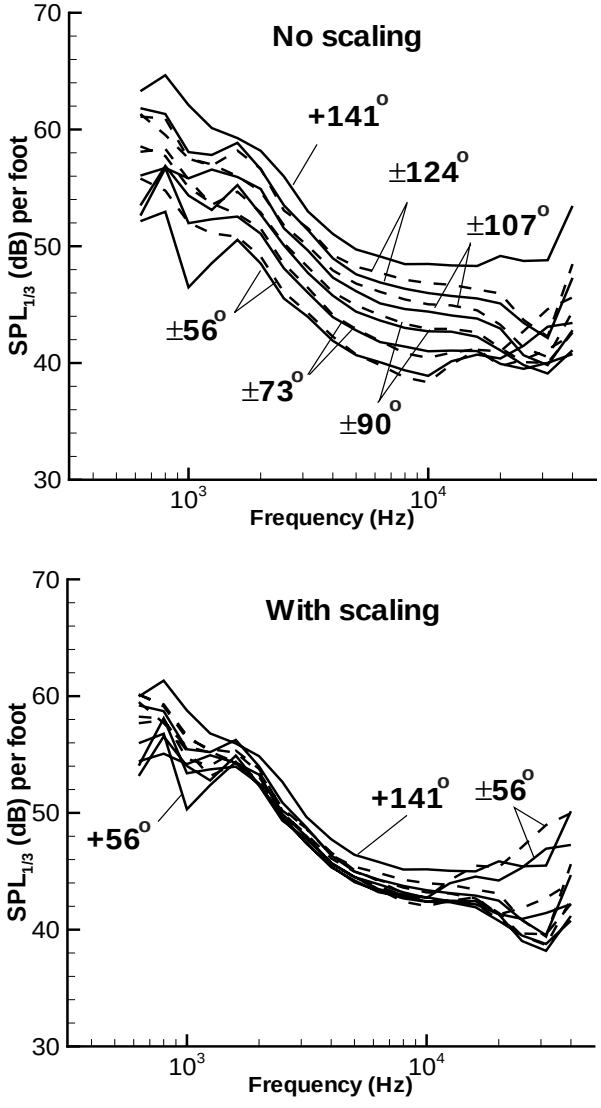

Figure 18. TE noise directivity. M=0.17; airfoil at —1.2 angle of attack; TE configuration #7; #90 grit on LE.
——— SADA at positive elevation angles;
– – – – – – SADA at negative elevation angles.

For the rod test case, with its strong line-like source and limited noise contamination, the spectra were found to scale well over the entire frequency range with the exception of the second spectral peak around 10 kHz where the noise seems to radiate with a different directivity.

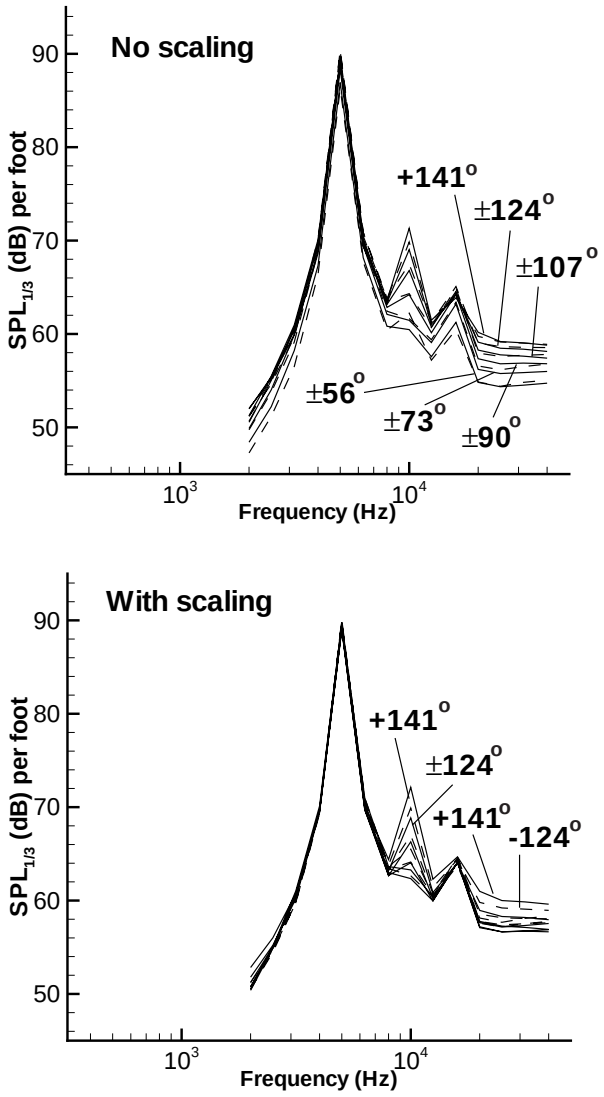

Figure 19. TE noise directivity. M=0.17; smooth 0.093Ó diameter rod. —— SADA at positive elevation angles; ------ SADA at negative elevation angles.

CONCLUSIONS

The use of a directional microphone array method for the measurement of TE noise and other line-source noise is presented and tested. The array used is the Small Aperture Directional Array (SADA). Also examined is a second measurement technique (COP method) that is based on the cross-spectral analysis of output signals from a pair of microphones placed around the test model. The capabilities of the two methods were evaluated via measurements of TE noise from a NACA 63-215 airfoil model and noise from cylindrical rods.

It is found that the SADA array approach produced a greater understanding and a more quantitative determination of TE noise over a broader frequency range than the COP method. For the present model, the SADA method is well suited for the study of distributed sources such as TE noise. Except when LE noise interfered with the TE noise measurements due to side lobe noise contamination, the array method provided a noise distribution contour mapping that clearly defined the TE noise region. Spectral presentation employing the array results, provided a common basis for comparing with spectra from the COP method and prediction.

The COP method is more restrictive in its use than the array approach. Even though restrictive, the method is attractive because of its equipment and analysis simplicity. The source must be a line source of well-defined character that can be modeled into the COP processing method. For the present TE noise and small rod noise sources, the source generally meets the single line dipole distribution requirement. It is found that for the present models, the COP works well over a frequency range that is validated by the examination of the fidelity of the cross-spectral phase.

The spectra determined from both the array and COP methods were compared to predicted TE noise using a semi-empirical airfoil self-noise prediction code. Measured boundary layer values were used. Agreement was found over broad frequency ranges for TE noise due to boundary layer turbulence and TE bluntness. Largest differences between measurement and prediction were found at the highest frequencies.

An important strength of the SADA array method is clearly shown in the present study. The SADA array method defines both the TE noise (related to the classical TE pressure scatter problem) and LE noise (related to boundary layer tripping grit). The COP method only perceives the TE noise. The array is able to quantify more of the total noise output of a model.

ACKNOWLEDGMENTS

The authors wish to thank their colleague William M. Humphreys for his valuable assistance in the data processing. They also gratefully acknowledge Daniel J. Stead of Lockheed-Martin for the measurement and processing of the near-wake velocity data.

REFERENCES

1. Crighton, D. G., "Aeroacoustics of Flight Vehicles: Theory and Practice, Volume 1: Noise Sources", NASA Reference Publication 1258, August 1991.

2. Schlinker, R. H., "Airfoil Trailing Edge Noise measurements with a directional microphone", AIAA Paper 77-1269, 1977.

3. Yu, J. C. and Joshi, M. C., "On Sound Radiation from the trailing Edge of an Isolated Airfoil in a Uniform Flow", AIAA Paper 79-0603, 1979.

4. Brooks, T. F. and Hodgson, T. H., "Trailing Edge Noise Prediction from Measured Surface Pressures", *Journal of Sound and Vibration*, Volume 78, Number 1, pp.69-117, 1981.

5. Gershfeld, J., Blake, W. K. and Knisely, C. W., "Trailing Edge Flows and Aerodynamic Sound", AIAA Paper 88-3826.

6. Soderman, P. T. and Noble, S. C., "A Four-Element End-Fire Microphone Array for Acoustic Measurements in Wind Tunnels", NASA Technical Memorandum X-62, 331, January, 1974.

7. Soderman, P. T. and Noble, S. C., "Directional microphone Array for Acoustic Studies of Wind Tunnel Models", AIAA paper 74-640, 8th AIAA/AT Conference, Bethesda, MD, July 8-10. 1974.

8. Marcolini, M. A. and Brooks, T. F., "Rotor Noise measurement using a Directional Microphone array", *Journal of the American Helicopter Society*, Vol. 37 (2), pp. 11-22, April, 1992.

9. Bent, P. H., Guo, Y., Horne, C. W. and Watts, M. E., "Airframe Noise Scaling and Source Localization", Noise-Con 96, pp. 145-150, Seattle, Washington, September 29 - October 2, 1996.

10. Meadows, K. R., Brooks, T. F., Humphreys, W. M., Hunter, W. W., and Gerhold, C. H., "Aeroacoustic Measurements of a Wing-Flap Configuration", AIAA Paper 97-1595, 1997.

11. Van der Wal, H. M. and Sijtsma, P., "Flap Noise Measurements in a Closed Wind tunnel with a Phased Array", AIAA Paper 2001-2170, 7th AIAA/CEAS Aeroacousics Conference, Maastricht, The Netherlands, May 28-30, 2001.

12. Brooks, T.F. and Humphreys, Jr., "Flap Edge Aeroacoustic Measurements and Predictions", AIAA Paper No. 2001-1975, 2001.

13. Oerlemans, S., Schepers, J. G., Guidati, G. and Wagner, S., "Experimental Demonstration of Wind Turbine Noise Reduction Through Optimized Airfoil Shape and Trailing-Edge Serrations", European Wind Energy Congress, Copenhagen, Denmark, July 2-6, 2001.

14. Mosher, M., "Phased Arrays for Aeroacoustic Testing: Theoretical Development," AIAA Paper 96-1713, 2nd AIAA/CEAS Aeroacoustics Conference, state College, PA, May 6-8, 1996.

15. Brooks, T.F. and Humphreys, W.M., Jr., "Effect of Directional Array Size on the Measurement of Airframe Noise Components", AIAA Paper No. 99-1958, 1999.

16. Storms, B. L., Ross, J. C., Horne, W. C., Hayes, J. A., Dougherty, R. P., Underbrink, J. R., Scharpf, D. F., and Moriarty, P. J., "An Aeroacoustic Study of an Unswept Wing with a Three-Dimensional High-Lift System," NASA TM-1998-112222, 1998.

17. Humphreys, W. M., Brooks, T. F., Hunter, W. W. and Meadows, K. R., "Design and Use of Microphone Directional Arrays for Aeroacoustics Measurements", AIAA Paper 98-0471, 1998.

18. Brooks, T. F., Pope, D. S., and Marcolini, M. A., "Airfoil Self-Noise and Prediction", NASA Reference Publication 1218, July, 1989.

19. Johnson, D. H. and Dugeon, D. E., *Array Signal Processing*, Prentice Hall, 1993.

20. Amiet, R. K.,"Refraction of Sound by a Shear layer", *Journal of Sound and Vibration*, Vol. 58 (3), pp. 467-482, Sept. 1978.

21. Mendoza, J. M., Brooks, T. F. and Humpfreys, W. M., "Aeroacoustic Measurements of a High-Lift Wing/Slat Model", AIAA paper 2002-2604, 8th AIAA/CEAS Aeroacoustics Conference, Breckenridge, CO., June 17-19, 2002.

22. Bendat, J. S. and Piersol, A. G., "Engineering Applications of Correlation and Spectral analysis", John Wiley & Sons, 1980.

23. Brooks, T. F. and Marcollini, M. A., "Scaling of Airfoil Self Noise Using Measured Flow Parameters", *AIAA Journal*, Vol.23, 1985.

24. Brooks, T. F. and Marcollini, M. A., "Airfoil Tip Vortex Formation Noise", *AIAA Journal*, Vol.24, 1986.

25. Brooks, T. F., Marcollini, M. A. and Pope, D. S., "Airfoil Trailing edge Flow Measurements", *AIAA Journal*, Vol.24, 1986.